

Bi-global crossplane stability analysis of high-speed boundary-layer flows with discrete roughness

Gordon Groskopf, Markus J. Kloker and Olaf Marxen

Abstract Bi-global secondary linear stability theory (B-SLST) is applied to a laminar Mach 4.8 flat-plate boundary-layer flow altered by discrete roughness elements, roughly 0.5 undisturbed boundary-layer thicknesses high. The steady primary state gained by DNS with the immersed-boundary technique shows a counter-rotating vortex pair (CVP) generating a low-speed streak in the roughness' centerline wake. The resulting wall-normal and spanwise shear promotes 1st-mode instability, increasing the growth rate roughly by a factor of four. Two modes are obtained: a symmetric y -mode and an antisymmetric z -mode. A comparison with an unsteady DNS, where time-periodic 2-d perturbations are introduced upstream of the roughness, shows well matching growth rates and amplitude distribution of the y -mode.

1 Introduction

If a flow is dominated by localized structures in its crosscut, e.g., by longitudinal vortices, strong wall-normal and spanwise gradients exist, and thus, the (secondary) instability is localized in the flow crosscut rather than monoharmonic, like it is assumed in classical SLST. An eigenvalue problem with 2-d eigenfunctions results, i.e., we have a bi-global approach (B-SLST). See [7], [4] and [1] for B-SLST applied to incompressible flows with (crossflow-)vortices.

In high-speed flows laminar-turbulent transition of the boundary layer is often induced or promoted by discrete 3-d roughness. B-SLST can be used to identify instabilities in the wake of roughness elements that is dominated by a longitudinal CVP and a subsequently developing low-velocity streak. The same holds for setups of effusion cooling (see, e.g., [6]). The modifying mechanisms for disturbance receptivity and instability caused by 3-d roughness elements are still unclear, depending on their shapes, heights, distance, etc. Recently, [2] also started B-SLST work for the investigation of devices to trip hypersonic laminar boundary layers.

2 Bi-global secondary linear stability theory & numerics

The applied B-SLST solver is based on the compressible 3-d Navier-Stokes equations in primitive variables: $\mathbf{q} = [\rho \ u \ v \ w \ T]^T$, where density, velocity components in directions x (streamwise, u), y (wall-normal, v), z (spanwise, w), and temperature are

Gordon Groskopf, Markus J. Kloker
Universität Stuttgart, Germany, e-mail: (last name)@iag.uni-stuttgart.de

Olaf Marxen
Stanford University, United States, e-mail: olaf.marxen@stanford.edu

split into steady primary-state (index 1) and unsteady perturbation (superscript $'$): $\Phi(x, y, z, t) = \Phi_1(x, y, z) + \Phi'(x, y, z, t)$. A calorically perfect-gas flow with constant Prandtl number is assumed at this stage. The usual assumptions and requirements for (primary) linear stability theory are applied. Specialties are:

- B-SLST allows $v_1 \neq 0$ as long as it does not contribute to boundary-layer growth. Hence the mean value or, in spectral space, the zeroth mode of v_1 is zero.
- In the modal perturbation ansatz $\mathbf{q}'(x, y, z, t) = \hat{\mathbf{q}}(y, z) \cdot e^{i(\alpha x - \omega t)}$, $\hat{\mathbf{q}}(y, z)$ is the complex 2-d amplitude distribution; α and ω describe the spatial wavenumber in x -direction and the frequency, respectively.

Thus a linear eigenvalue problem results for the temporal approach ($\alpha = \alpha_r$, $\omega = \omega_r + i \cdot \omega_i$), solved using the implicitly restarted Arnoldi method (IRAM) implemented in ARPACK (see [5]). Spatial eigenvalues can be obtained by either Gaster's transformation or an iteration of the general solution to $\omega_i \rightarrow 0$. Eighth-order finite differences are used for the primary state as well as for the perturbation. Near boundaries in y -direction the order is reduced to four. The primary flow and perturbation are assumed to be periodic in z . At the wall the no-slip condition is prescribed. The temperature perturbation is set to zero. In the freestream all perturbations are assumed to vanish. More details can be found in [3]. Despite the assumption $\frac{\partial}{\partial x} \equiv 0$, all variables are taken here directly from the DNS of the primary flow.

3 Primary state

A roughness element is placed on an adiabatic flat plate using the immersed boundary method (IBM) in the DNS ([3], [8], [9]). Note that the stability results rely on the primary state, demanding a careful temporal as well as spatial convergence study in computing the primary flowfield.

The investigated roughness configuration is a square-box type element in a cold, supersonic flow with $Ma_\infty = 4.8$, $T_\infty = 55.4$ K ($T_0 = 311$ K). Prandtl number and adiabatic exponent are fixed to 0.71 and 1.4, respectively. The Reynolds number based on the reference length L^* is $Re = 10^5$, thus $\rho_\infty^* L^* = 4.87 \cdot 10^{-4} \frac{\text{kg}}{\text{m}^2}$ with $\mu_\infty^* = 3.49 \cdot 10^{-6} \frac{\text{Ns}}{\text{m}^2}$ and $u_\infty^* = 716.15 \frac{\text{m}}{\text{s}}$. The element is placed at $x = 15.0$, $R_x = 1225$, downstream of the leading edge of the plate with a height $h = 0.55 \delta_u$ of the unperturbed flow at that position. Fig. 1 and Table 1 show the setups.

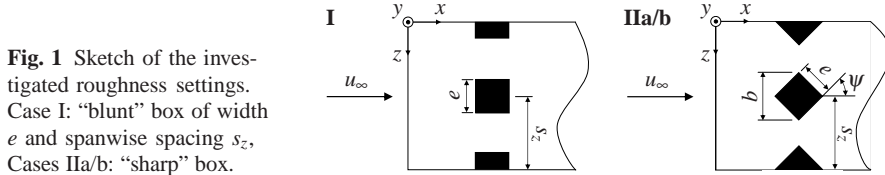


Fig. 1 Sketch of the investigated roughness settings. Case I: "blunt" box of width e and spanwise spacing s_z , Cases IIa/b: "sharp" box.

Table 1 Overview of box settings for the investigated cases. Symbols refer to Fig. 1.

case		e	b	s_z/b	h	ψ
I	blunt	$2.2\delta_u$	$2.2\delta_u$	3.0	$0.55\delta_u$	0°
IIa	sharp	$2.2\delta_u$	$2.2\sqrt{2}\delta_u$	2.1	$0.55\delta_u$	45°
IIb	small sharp	$1.1\sqrt{2}\delta_u$	$2.2\delta_u$	3.0	$0.55\delta_u$	45°

Fig. 2 indicates the trailing vortices. Between the inner counter-rotating vortices low-momentum fluid is lifted up towards the boundary-layer edge, forming a low-

speed streak behind the element. The lift-up of vortices in streamwise direction additionally increases the shear near the boundary-layer edge providing the base for increased instability. Cases IIa/b differ from case I in spanwise spacing of the vortices. The u -amplitude of the velocity streak is shown in Fig. 3. Compared to the decaying vorticity ω_x of the CVP in streamwise direction it persists along x . The reversal of flow in the near-wake region possibly causing absolute or global instability plays no significant role. Downstream the roughness element the streamwise derivative of the u -velocity is more than one order of magnitude lower than the crosswise derivatives, justifying the B-SLST assumptions.

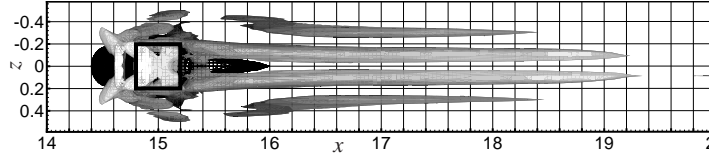
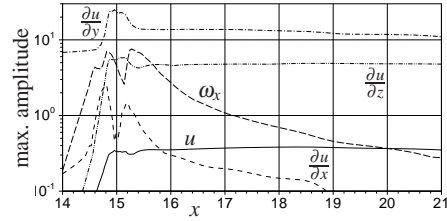


Fig. 2 Top view of vortex structures in the wake of the roughness element for case I (λ_2 criterion, $\lambda_2 = -0.04$). Flow is from left to right. The shading indicates the height y of the λ_2 -isosurface above the wall (the lighter the higher). The meshed (black) isosurface shows the dimension of the recirculation zones ($u < 0$). Thick solid lines show the borders of the roughness elements.

Fig. 3 Maximum amplitude of 3-d u -velocity deformation of the flow, streamwise vorticity ω_x and u -velocity gradients in $(y-z)$ -planes over streamwise direction x for case I.



4 Results

The B-SLST analysis is carried out in $(y-z)$ -crosscut planes at various x -positions in the wake of the roughness element. The spatial growth rates are obtained applying Gaster's transformation according to [4], see also [1]. Two relevant instability modes have been found. Called y -(or even) mode and z -(or odd) mode they are related to the wall-normal or the spanwise gradients in the flowfield, respectively.

Streamwise analysis As a first guess $\alpha_{r,t}$ is chosen corresponding to the most amplified 1st-mode instability. The wavelength is about $6\delta_u \leq \lambda_x \leq 10\delta_u$, hence we set $\alpha_{r,t} = 5.0$, equivalently $\alpha_{r,t}\delta_u = 1.0$. Spatial amplification rates $\alpha_{i,S}$ and corresponding N factors for the most amplified y - and z -mode of the investigated cases are shown in Fig. 4. The frequency is a result of the theory and thus, varies along x (max. $\Delta\omega_{r,t} = \pm 10\%$). The maximum amplification rate of both modes is of similar magnitude for all cases, and reaches roughly four times the maximum primary amplification rate of the flat-plate flow at $x = 18$ ($R_x = 1341$). However, the characteristics of y - and z -mode differ. While the y -mode exhibits high amplification in the near wake and decays rather quickly in streamwise direction, the z -mode reaches its peak amplification further downstream, and high values of the growth rate seem to persist downstream, which apparently is consistent with $\frac{\partial u}{\partial z}$ of the primary state (see

Fig. 3). Remarkably, the z -mode of case IIb already shows high amplification in the near wake. Up to $x = 21$ the largest integral growth is observed for the y -mode of cases I and IIa (Fig. 4, right). Recall that $N = \int \alpha_{i,S} dx$, and $A/A_0 = e^N$. Assuming that the growth rates of the z -modes persist, their integral growth will exceed the y -modes already slightly further downstream. We note that the analysis at streamwise stations upstream the element did not show notable amplifications.

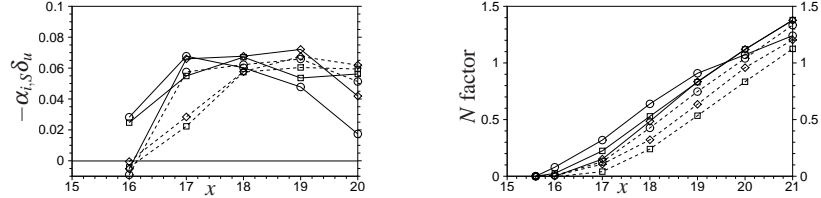


Fig. 4 Spatial amplification rates over streamwise direction x (left) and corresponding N factors (right) for the most amplified y -mode (solid) and z -mode (dashed) at x -positions indicated by symbols. Wavenumber $\alpha_{r,S} \delta_u = \alpha_{r,t} \delta_u = 1.0$. Case I: squares, case IIa: diamonds, case IIb: circles.

Eigenfunctions The moduli $\Phi' = |\hat{\Phi}|$ of the complex eigenfunctions for case I (Fig. 5) are normalized by the highest value occurring in the u' -distribution. The phase distribution for p shows that the y -mode is symmetric to $z = 0$ while the z -mode is antisymmetric. All shown distributions share that the maxima are located above the sonic line in the supersonic regime at the edge of the deformed boundary layer. For more details about the eigenfunctions, especially regarding the differences between the three investigated roughness setups, see [3].

Wavenumber dependence A scan over $\alpha_{r,t}$ has been carried out at $x = 18$. The covered range is $0.25 \leq \alpha_{r,t} \delta_u \leq 3.0$. Results are displayed in Fig. 6. The z -mode is most amplified for a wavenumber smaller than 1. The maximum amplification rate of the z -modes is virtually identical for the three investigated cases. Apart from that, the curves for identical modes show similar behavior. The value $\alpha_{r,t} \delta_u = 3.0$ is typically associated with the second-/acoustic mode having a streamwise wavelength of about $\lambda_x = 2\delta_u$ in a supersonic flat-plate boundary-layer flow. But amplification for this wavenumber was not found in any case for any mode. We note that the 2-d second mode is not amplified in the roughnessless flow at this position either.

Comparison with unsteady DNS Concurrent to the theoretical stability analysis, a disturbance calculation using the DNS has been set up for case I. Disturbances are forced using monofrequent 2-d blowing and suction within a spanwise disturbance strip at the wall, a short distance upstream the roughness element. The frequency is $\omega_{r,DNS} = 4.1$, obtained by stability analysis for $\alpha_{r,t} \delta_u = 1.0$ at $x = 18$. Due to the symmetric forcing only excitation of symmetric modes, i.e. the y -mode, could be expected.

Fig. 7 displays beatings caused by superposition of multiple eigenmodes of identical frequency but slightly different streamwise wavenumbers. A comparative superposition of the amplitude growth from DNS with the N -factor development from stability theory (Fig. 7) shows good agreement.

The u' -amplitude distribution extracted from DNS at $x = 18$ and normalized by the maximum value in the crosscut shows very good agreement with the B-SLST re-

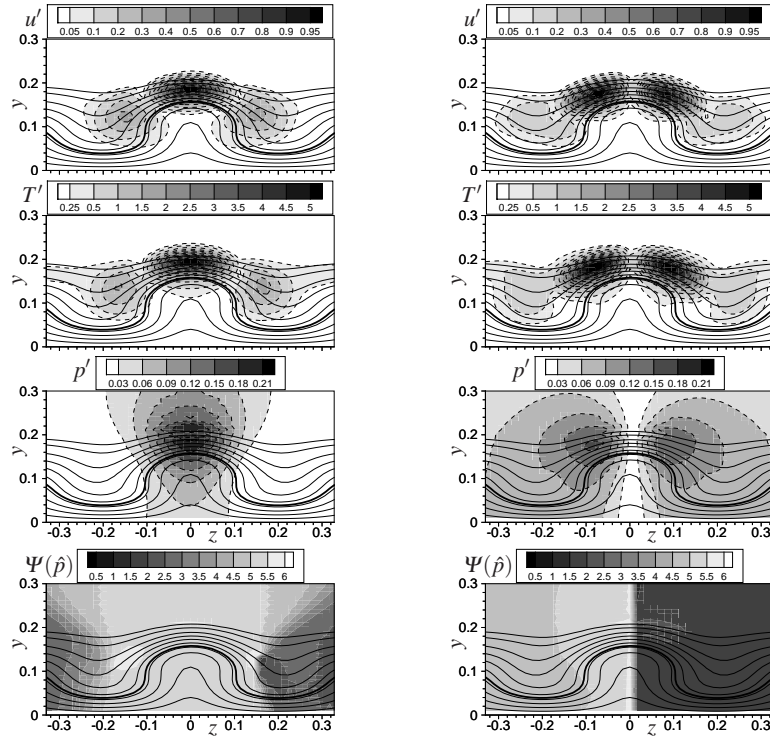


Fig. 5 Eigenfunctions of u' , T' and p' . Contours show the modulus of perturbation amplitude $\Phi' = |\hat{\Phi}|$. y -mode (left) and z -mode (right) are displayed at position $x = 18.0$ for case I. Thin solid lines are isolines of u beginning with $u = 0.1$ near the wall and ending with $u = 0.95$. Thick solid lines mark the sonic line. Last row: Phase distribution $\tan \Psi(\hat{p}) = \frac{\hat{p}_i}{\hat{p}_r}$ for the p' eigenfunctions.

Fig. 6 Spatial amplification rates over given streamwise wavenumbers indicated by symbols for the most amplified y -mode (solid) and z -mode (dashed) at $x = 18.0$. Case I: squares, case IIa: diamonds, case IIb: circles.

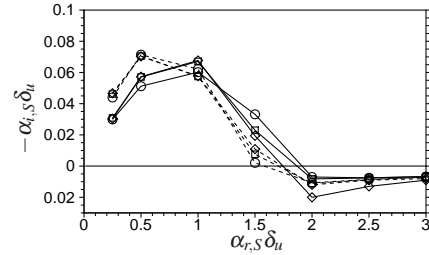
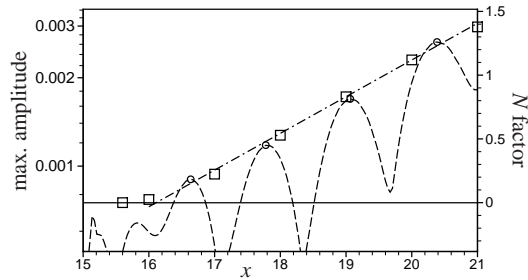


Fig. 7 Streamwise amplitude development (max. over y and z) for y -mode (long dash) from unsteady DNS of case I (log scale), regression line (dash-dot) based on maxima (circles) and N -factor development from B-SLST (squares) for y -mode of case I (linear scale).



sult, especially the position of amplitude maxima is excellently reproduced (Fig. 8).

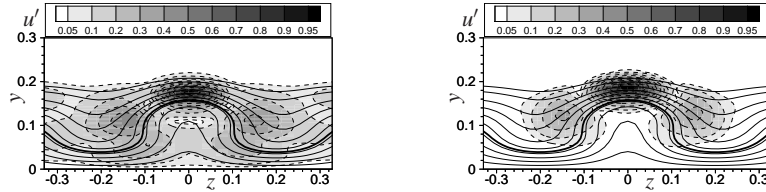


Fig. 8 Comparison: DNS vs. B-SLST. y -mode for case I at position $x = 18.0$. Left: normalized u -velocity perturbation amplitude u' from DNS. Right: Contour of modulus of normalized u -perturbation amplitude $u' = |\hat{u}|$ from theory. Thin solid lines are isolines of u beginning with $u = 0.1$ near the wall and ending with $u = 0.95$. Thick solid lines mark the sonic line.

5 Conclusions

A Mach 4.8 laminar boundary-layer flow altered by discrete 3-d roughness has been investigated regarding its instability behavior. The square-box type roughness element is found not to cause sudden bypass-transition. The horseshoe vortex plays virtually no role for the instability increase. Neither was the recirculation found to cause absolute instability. Rather, the inner pair of counter-rotating vortices past the element and the resulting low-speed streak in the downstream centerline cause a pronounced convective instability with a growth rate roughly four times the primary-instability value without roughness. For the velocity streak, relevant growth downstream the roughness element was not found. So the roughness acts as an amplifier for 1st-mode instabilities. According to the B-SLST the sharp-type roughness arrangement is slightly more dangerous to laminar flow than the blunt setting. Generally, y - and z -mode exhibit similar amplification rates. But as the amplification of the z -mode persists further downstream, this mode might be more important for transition. It also has a somewhat smaller streamwise wavenumber, between 0.5 and 1.0, non-dimensionalized by the boundary-layer thickness, for the most amplified modes. The existence of the y -mode could be confirmed by an unsteady DNS, and comparison of the disturbance shapes shows excellent agreement. The growth rates could only be compared approximately, but also good agreement was found.

References

1. BONFIGLI G. & KLOKER M. J. 2007 Secondary instability of crossflow vortices: validation of the stability theory by direct numerical simulation. *J. Fluid Mech.* **583**, 229–272.
2. CHOUDHARI M. M., LI F. & EDWARDS J. 2008 Advanced stability analysis pertaining to roughness effects on laminar-turbulent transition in hypersonic boundary layers. *NASA AAP Quarterly Highlights* Hypersonics Project, Vol. 2, No. 2, April 2008.
3. GROSCHOPF G., KLOKER M. J. & MARXEN O. 2008 Bi-global secondary stability theory for high-speed boundary-layer flows. In *Proceedings of the 2008 Summer Program*, CTR, Stanford, Calif., July 6–August 1.
4. KOCH W., BERTOLOTTI F. P., STOLTE A. & HEIN S. 2000 Nonlinear equilibrium solutions in a three-dimensional boundary layer and their instability. *J. Fluid Mech.* **406**, 131–174.
5. LEHOUCQ R. B., SORESENSEN D. C. & YANG C. 1998 *ARPACK User's Guide*. SIAM, Philadelphia, Penn.
6. LINN J. & KLOKER M. J. 2008 Numerical investigations of film cooling and its influence on the hypersonic boundary-layer flow. *NNFM 98*, final reviewed papers of the HGF virtual institute RESPACE Key technologies for re-usable space systems (ed. Guelhan, A.), Springer-Verlag, Berlin, 151–169.
7. MALIK M. R. & CHANG C.-L. 1994 Crossflow disturbances in three-dimensional boundary layers: nonlinear development, wave interaction and secondary instability. *J. Fluid Mech.* **268**, 1–36.
8. MARXEN O. & IACCARINO G. 2008 Numerical simulation of the effect of a roughness element on high-speed boundary layer instability. Thirty-eighth *AIAA Fluid Dynamics Conference & Exhibit*, 23–26 June / Seattle, Wash. AIAA Paper 2008-4400.
9. NAGARAJAN S., LELE S. K. & FERZIGER J. H. 2003 A robust high-order method for large eddy simulation. *Physics of Fluids A* **4** (4), 710–726.